Title: Ablation of Sam50 is associated with fragmentation and alterations in metabolism in human myotubes

Authors: Zer Vue[1*], Chia Vang[1*], Kit Neikirk[1*], Edgar Garza-Lopez[2], Jian-qiang Shao[3], Margaret Mungai[2], Larry Vang[1], Heather Beasley[1], Andrea G. Marshall[1], Amber Crabtree[1], Dominique Stephens[1], Melanie McReynolds[5,6], Sandra A. Murray[7], Prasanna Katti[13], Steven Damo[14], Jennifer A. Gaddy[11,12*], Antentor Hinton, Jr[1*]

[1] Department of Molecular Physiology and Biophysics, Vanderbilt University, Nashville, TN, 37232, USA
[2] Department of Internal Medicine, University of Iowa, Iowa City, IA, 52242, USA
[3] Central Microscopy Research Facility, University of Iowa, Iowa City, IA, 52242, USA.
[4] Microscopy and Cell Analysis Core Facility, Mayo Clinic, Rochester, MN, 55905, USA
[5] Department of Biochemistry and Molecular Biology, Pennsylvania State University, University Park, PA
[6] Huck Institutes of the Life Sciences, Pennsylvania State University, University Park, PA
[7] Department of Cell Biology, School of Medicine, University of Pittsburgh, Pittsburgh, PA, 15260, USA
[8] Department of Pediatrics, Div. of Cardiology, St. Louis University School of Medicine, St. Louis, MO, 63104, USA
[9] Department of Medicine, Baylor College of Medicine, Houston, TX, 77001
[10] Department of Pathology, Carver College of Medicine, University of Iowa, Iowa City, IA, 52242, USA
[11] Division of Infectious Diseases, Vanderbilt University School of Medicine, Nashville, TN, 37232, USA
[12] Tennessee Valley Healthcare Systems, U.S. Department of Veterans Affairs, Nashville, TN, 37212, USA
[13] National Heart, Lung and Blood Institute, National Institutes of Health, Bethesda, MD, United States
[14] Department of Life and Physical Sciences, Fisk University, Nashville, TN, 37208, USA
*-Indicates Equal Authorship
Corresponding Authors:
Antentor O. Hinton, Jr, PhD
Vanderbilt School of Medicine Basic Sciences
antentor.o.hinton.jr@Vanderbilt.edu

Keywords: 3D reconstruction, mitochondria, SAM complex, Sam50, MICOS

Abstract: The Sorting and Assembly Machinery (SAM) Complex functions in the assembly of β-barrel in the mitochondrial membrane. The SAM complex is made up of three subunits,

Sam35, Sam37, and Sam50. While both Sam35 and Sam37 are peripheral membrane proteins that are not required for survival, Sam50 interacts with the MICOS complex to connect the inner and outer mitochondrial membranes and forms the mitochondrial intermembrane space bridging (MIB) complex. Specifically, Sam50 stabilizes the MIB complex for protein transport, respiratory chain complex assembly, and cristae integrity regulation. To structurally form and sustain the cristae, the MICOS complex assembles at the cristae junction and binds directly to Sam50. However, the role of Sam50 in overall mitochondrial structure and metabolism in skeletal muscle remains unclear. Here, we use SBF-SEM and Amira software perform 3D renderings of mitochondria and autophagosomes in human myotubes. Beyond this, Gas Chromatography-Mass Spectrometry-based metabolomics was utilized to interrogate differential changes of the metabolites in wild-type (WT) and *Sam50* deficient myotubes. Ablation of *Sam50*, revealed increases in ß-Alanine, propanoate, and phenylalanine, and tyrosine metabolism. Additionally, we observed that mitochondrial fragmentation and autophagosome formation was increased in *Sam50*-deficient myotubes compared to control myotubes. Beyond this, the metabolomic analysis revealed an increase in amino acid metabolism and fatty acid metabolism. XF24 Seahorse Analyzer shows that oxidative capacity is further impaired upon ablation of *Sam50* in both murine and human myotubes. Together, these data suggest Sam50 is critical for establishing and maintaining mitochondria, mitochondrial cristae structure, and mitochondrial metabolism.

Introduction:

Mitochondria are generally associated with their bioenergetic roles in the cell, as double-membraned organelles which carry out respiration (1,2). Beyond this, mitochondria also carry out additional functions through calcium homeostasis, apoptotic processes, and various disease progressions (2,3). In general, mitochondria may offer clues towards the treatment of many common diseases. For example, reactive oxidative species may alter various other functions of mitochondria including the crucial role of ATP production, which may be linked to diabetes (4). As a mechanism to protect against the dysregulation of mitochondria in neurodegenerative diseases, autophagy commonly occurs to recycle dysfunctional mitochondria (5). Beyond this, mutations or changes in the function of the mitochondrial DNA (mtDNA) can result in altered mitochondrial function; this can have consequences on insulin production, lead to hypertension, and ultimately be related to the progression of Diabetes Mellitus (6,7). Increasingly, research has focused on the complex relationship between mitochondrial structure and function (8). Although less understood, various mitochondrial ultra-structures are also involved in chemical pathways to regulate calcium, potassium, and other biomolecules (9). Thus, the prospect of understanding how changes in mitochondrial structure may affect metabolism and macro autophagy remains pertinent for discovering treatments for the leading causes of death in the world (10).

Critical to understanding the bi-membraned structure of mitochondria are the folds of the inner membrane known as cristae (11). Cristae occur in the mitochondria to maximize the amount of oxidative phosphorylation that may occur relative to internal volume (11). Beyond

these internal junctions, mitochondria gross structure is also heavily affected by independent dynamics of fusion and fission which regular various mitochondrial phenotypes which range from the typical spherical to stress-states including megamitochondria and donut-shaped (8,12). GTPase Mitofusin-1 (Mfn1) and Mitofusin-2 (Mfn2), for the outer membrane, and Optic atrophy 1 (Opa1), for the inner membrane, regulate the mitochondrial fusion process (11,13,14). Opa1 has been shown to be linked to mitochondrial fragmentation while also affecting cristae dimensions, shapes, and size (15). Specifically, Opa1 exists in two principal isoforms, the short and long forms, which have been theorized to be responsible for cristae and mitochondrial dynamics, respectively (16). This is relevant as the distance between cristae and outer membrane, for example, is important in establishing the health of mitochondria (17). Thus, understanding the mechanisms of how modulators of cristae affect overall mitochondrial structure remains important.

As such, mitochondria can be classified into several sublayers (Figure 1). The inner membrane of the mitochondria, at cristae junctions, the has mitochondrial contact site and cristae organizing system (MICOS) complex (15,18,19). These are bonded to sorting and assembly machinery (SAM) complex (18). Together, these two components interact and connect the inner and outer mitochondrial membranes to form the mitochondrial intermembrane space bridging (MIB) complex (18). These genes are important in organizing and structuring the mitochondria to allow for maximum and efficient respiration and ATP generation (20). The MICOS complex, SAM complex, and OPA1 can all affect the dynamics of the cristae in varying ways (15,18,21,22). OPA1 is important in promoting the formation of a cristae sheet at ATP synthase by decreasing the gap between the two sides of the inter-membrane space of cristae (15). On the other hand, the MICOS genes interact with the SAM genes to assemble β-barrel proteins and maintain contact between the outer and inner membranes (15,22,23). These all are necessitated in maintaining the overall shape and distances in mitochondrial networks. Overall, cristae membranes are critical in maintaining and hosting electron transport chain protein complexes and the ATP synthase dimers, which are necessary for the production of ATP through oxidative phosphorylation (11,21). However, given the critical relationship observed between mitochondrial morphology and function; affecting the structure of mitochondria through the knockout of SAM-associated genes must be elucidated to better understand the functional impact on ultrastructure and morphology.

While the functions of the SAM complex may easily be considered as a subset of the MIB complex, the SAM complex remains an interesting target distinct from the MICOS complex. The SAM complex is made up of three subunits, Sam35, Sam37, and Sam50 (24). While both Sam35 and Sam37 are peripheral membrane proteins that are not required for survival, the central component, Sam50, a 7–8 nm diameter β-barrel channel, interacts with the MICOS complex to modulate protein transport and mitochondrial morphology (18,22,23,25). Specifically, Sam50 stabilizes the MIB complex for protein transport, respiratory chain complex assembly, and cristae integrity regulation (26). In this way, it is understood that to structurally form and sustain the cristae, proteins of the MICOS complex assemble at the cristae junction and

bind directly to Sam50 (20,22,27). Considering the entire MIB complex, Sam50 is considered to be among the most important protein, alongside members of the MICOS complex Mitofilin and Chchd3, for proper mitochondria structure and function (28). This central role is clearly elucidated, as loss of *Sam50* can result in diminished cristae count, reduced cristae dynamic events, abnormal cristae, and a lack of cristae junctions, the sites at which cristae are tethered to the mitochondrial inner boundary membrane (15). However, mitochondrial dynamics in 3D upon loss of *Sam50* is not yet well understood, and the potential implications of changes in 3D structure on mitochondrial function and metabolism remains a gap in the literature.

While 2D microscopy techniques allow for the viewing of typical tubular mitochondria, phenotypes of mitochondria are changed in different types of tissues and disease states (8,29,30). Mitochondrial swelling can occur as a response to dysregulation of ion homeostasis (31), while toroid mitochondria can arise in a calcium-dependent manner in stress states (32). Through fusion and fission dynamics, it is understood that mitochondria can respond to cellular stress to balance factors including volume, which typically allows for greater ATP generation, and surface area, which typically allows for organelle-to-organelle contacts which are crucial for extraneous processes such as calcium homeostasis (8,33,34). However, 3D microscopy techniques are required for an understanding of many of the diverse phenotypes which mitochondria may display.

This study specifically examined the metabolomics of the knockdown of *Sam50* in murine and human myotubes. For the knockout of genes, myotubes, derived from satellite cell fusion, have emerged as robust cellular models which mimic the properties found in skeletal muscle (35). Importantly, human and murine myotubes remain distinct, with separate phenotypes and metabolic progression (36). Therefore, human myotubes were *ex vivo* isolated from skeletal muscle biopsies and differentiated in multinucleated myotubes in culture (37). To measure structure, we used a mixed method approach utilizing principally serial block-face-scanning electron microscopy to allow for manual tracings to be performed on z-direction slices, known as orthos, which were then aligned in analysis software Amira (33), and reconstructed into 3D structures. SBF-SEM importantly allows for the ability to see mitochondrial networking, as it offers high x- and y- resolution. We also sought to compare differences in mitochondrial structure and function based on human myotubes to better elucidate if *Sam50* may have a differential role in these models. Beyond structural dynamics, we sought to combine how changes in mitochondrial morphology upon *Sam50*-deficinecy alters mitochondrial function and general biochemical pathways, which may offer further implications for therapeutical targets involved in *Sam50*.

Materials and Methods:

Mice Care:

All procedures for the care of mice were in accordance with humane and ethical protocols approved by the University of Iowa Animal Care and Use Committee (IACUC) following the National Institute of Health (NIH) Guide for the Care and Use of Laboratory Animals as

described previously[26]. Experiments utilized WT male C57Bl/6J mice housed at 22 °C on a 12-hour light, 12-hour dark cycle with free access to water and standard chow. Mice were anesthetized with 5% isoflurane/95% oxygen.

Murine and Human Myotube Isolation:

Satellite cell isolation was performed as previously described (38). Satellite cells from *Sam50* $^{fl/fl}$ mice were plated on BD Matrigel-coated dishes and activated to differentiate into myoblasts in Dulbecco's modified Eagle medium (DMEM)-F12 containing 20% fetal bovine serum (FBS), 40 ng/ml basic fibroblast growth factor, 1× non-essential amino acids, 0.14 mM β-mercaptoethanol, 1× penicillin/streptomycin, and Fungizone. Myoblasts were maintained with 10 ng/ml basic fibroblast growth factor and differentiated in DMEM-F12 containing 2% FBS and 1× insulin–transferrin–selenium when 90% confluency was reached. Three days after differentiation, myotubes were infected with an adenovirus expressing GFP-Cre to achieve *Sam50* deletion. Adenoviruses were obtained from the University of Iowa Viral Vector Core facility. Experiments were performed between 3 and 7 days after infection.

RNA Extraction and RT-qPCR

The RNeasy kit (Qiagen Inc) was used to purify it and it was subsequently quantitated by the absorbance at 260 nm and 280 nm using a NanoDrop 1000 (NanoDrop products, Wilmington, DE, USA) spectrophotometer. A High-Capacity cDNA Reverse Transcription Kit (Applied Biosciences, Carlsbad CA), was utilized for isolated RNA (~1 µg) reverse-transcription. SYBR Green (Life Technologies, Carlsbad, CA) (39) were used to perform real-time quantitative PCR (qPCR). Three samples for each qPCR (~50 ng) were placed in a 384-well plate that subsequently underwent qPCR in ABI Prism 7900HT instrument (Applied Biosystems). The specific cycle they underwent was: 1 cycle at 95°C for 10 min; 40 cycles of 95°C for 15 s; 59°C for 15 s, 72°C for 30 s, and 78°C for 10 s; 1 cycle of 95°C for 15 s; 1 cycle of 60°C for 15 s; and one cycle of 95°C for 15 s. Results were normalized to glyceraldehyde-3-phosphate dehydrogenase (*GAPDH*) and presented as relative fold changes.

Measurement of OCR Using Seahorse

Oxygen consumption rate was measured for *Sam50* KD fibroblasts using an XF24 bioanalyzer (Seahorse Bioscience: North Billerica, MA, USA), as previously described (38,40). Briefly, cells were plated at a density of 20×10^3 per well and differentiated for 3 days. For *Sam50* KO models, CRISPR/Cas9 for the KO was added as per the protocol above prior to plating. In XF□DMEM (supplemented with 1 g/L D-Glucose, 0.11 g/L sodium pyruvate, and 4 mM L-Glutamine), cells were incubated without CO_2 for 60 minutes. Cells have oligomycin (1 µg/ml), carbonyl cyanide 4-(trifluoromethoxy)phenylhydrazone (FCCP; 1 µM), rotenone (1 µM), and

antimycin A (10 μM) performed in that order while remaining in the XF-DMEM media. After measurement, cells were lysed accordingly to prior protocols (40), using 20 μl of 10 mM Tris with 0.1% Triton X-100 added at pH 7.4, and media replaced with 480 μl of Bradford reagent. Total protein concentration was then measured at an absorbance at 595 nm and used for normalization. For each sample, three independent experiments were performed for each condition with representative data from the replicates being shown.

Segmentation and Quantification of 3D SBF-SEM Images Using Amira

SBF-SEM ortho slices were 3D reconstructed using contour tracing (manual segmentation) in Amira to perform 3D reconstruction, as described previously (33,41). 300−400 slices ortho slices were transferred to Amira, and 50-100 serial sections were chosen, stacked, aligned, and visualized. A blinded individual familiar with organelle morphology traced structural features manually on sequential slices of micrograph blocks. Dots represent the total number of mitochondria surveyed, which varies.

Gas Chromatography-Mass Spectrometry (GC-MS) and Analyzing Metabolomic Data
Samples were extracted for metabolites and prepared as previously designed (42). TraceFinder 4.1 was used preloaded with standard verified peaks and retention times to to compare metabolite peaks in each sample against an in-house library of standards. to correct for drift over time by using QC samples, we used previously described protocols (43). All datas were normalized to an internal standard to control for extraction, derivatization, and/or loading effects.Metabolomic analysis was performed as described previously (42) using the web service MetaboAnalyst 5.0 (https://www.metaboanalyst.ca/MetaboAnalyst/ModuleView.xhtml, last accessed on 1 September 2022). All tests performed were using built in comparison, including one-way ANOVA and Fisher’s LSD multiple comparison test. The fold enrichment number was calculated by the observed hits by the expected hits, which were determined by MetaboAnalyst 5.0.

Data Analysis

In graphs, black bars represent the standard error, and dots represent individual data points. For data with only two groups, an unpaired, t-test was used, while if more than two groups were compared, ANOVA with Tukeys Post-hoc analysis was utilized. For both of these analyses, GraphPad Prism software package was used (La Jolla, CA, USA). A minimum threshold of $p < 0.05$ indicated a significant difference. Higher degrees of statistical significance (**, ***, ****) were defined as $p < 0.01$, $p < 0.001$, and $p < 0.0001$, respectively.

Results:

Loss of Sam50 causes Loss of Mitochondrial Size and Alterations in Morphology in Human Myotubes

We performed manual contour segmentation for 3D reconstruction (Figure 1). Across 10 myotubes for each experimental condition, sectioning was performed on 10 µm by 10 µm slices, with a z-directional depth of 300 µm. 50 ortho slices (Figure 2A-B) were surveyed and manual contour tracing was performed on each mitochondrion to perform 3D reconstructions of mitochondria (Figure 2A'-B'). This allowed for complete mitochondrial 3D structure to be observed (Figure 2A''-B''). Given that mitochondrial size is linked with respiratory efficiency (31), we first sought to understand how mitochondrial size may change.

We observed that mitochondrial fragmentation was increased in *Sam50*-deficient human myotubes compared to control myotubes (Figure 2C). Similarly, the area in 3D was also decreased upon Sam50 loss (Figure 2D). This mimicked a loss in perimeter (Figure 1E), reducing the total mitochondrion available for surface area. While this showed that mitochondria heavily lost size, we sought to understand also how morphology may have functional impacts on overall mitochondrial efficiency.

To begin with we showed mitochondrial from transverse (Figure 3A) and (Figure 3A') in control and in *Sam50*-deficent myotubes (Figure 3B-B'). From there, we sought to understand how mitochondrial sphericity changed, which showed that *Sam50*-deficiency causes an increase in sphericity indicating less complexity (Figure 3C). To further understand mitochondrial complexity, we measured mitochondrial complexity index which is a measure of surface area to volume ratio, which showed that mitochondria become significantly less complex upon loss of *Sam50* (34) (Figure 3D). This is further validated when we organized mitochondria by volume in a karo-type-like arrangement known as mito-otyping, which showed that mitochondria in control are highly elongated (Figure 3F). Upon loss of *Sam50*, generally mitochondria become less elongated, resulting in decreases in overall volume. Alongside changes in elongation, we also looked at mitochondrial complexity index, which is a measure of surface area to volume ratio, (Figure 3G). Together, these data suggest dysregulated mitochondrial structure. To investigate a potential concomitant change in cellular processes, we looked at autophagic machinery through previously validated techniques (44).

Increased Mitophagy Occurs Upon Loss of *Sam50* in Human Myotubes

Most abundantly, macroautophagy is the routine cellular mechanism for organelles, including mitochondria, through principally autophagosomes (5). Targeting of mitochondria in autophagy, known as mitophagy, can serve as a critical cellular response to reactive oxygen species or other forms of dysfunctional mitochondria; as such, mitophagy has been proposed as a key target in limiting the pathological progression of neurodegenerative diseases (5). *Sam50* may play a crucial role in the biochemical triggering of these mitophagy events. Of note *Sam50* interacts with autophagy receptor p62 (45). Beyond this, past research has also found that *Sam50* deficiency results in autophagic flux, with mtDNA protecting from complete mitochondrial

degradation (46). However, autophagy remains a dynamic process that may be more effectively studied using 3D reconstruction (44), and the effects of *Sam50*-deficiency on the structure of autophagic organelle machinery are poorly elucidated.

Here, again using 3D reconstruction from 10 µm by 10 µm slices obtained from 10 myotubes, with a z-directional depth of 300 µm, we surveyed 50 ortho slices (Figure 4A). Following manual segmentation of these 50 ortho slices, 3D renderings of autophagosomes were able to be created for control and *Sam50*-deficient human myotubes (Figure 4B-B'). We found that autophagosomes, when normalized to the same area regions of interests (ROI), were much higher in count upon loss of *Sam50* in human myotubes (Figure 4C). Beyond only count, the average volume of each autophagosome increases (Figure 4D). These increases in overall size can be illustrated when autophagosomes are organized on the basis of their volume (Figure 4E). This suggests larger autophagosomes that may be more active or have increased cargo loads. Together, these results show that autophagosome formation was increased in *Sam50*-deficient myotubes compared to control myotubes, suggesting an uptick in mitophagy.

Alterations of Mitochondrial Efficiency Occurs in *Sam50*-deficient Murine and Human Myotubes

From there, we turned our attention to understanding how these structural changes in mitochondria and recycling machinery affected the overall oxidative capacity of both human and murine myotubes. To do so, we used an XF24 Seahorse Analyzer which measures oxygen consumption rate (OCR) across various drug applications, which is analogous to mitochondrial oxidative photophosphorylation across several states in murine myotubes. To begin with we confirmed knockout of Sam50 in both murine and human myotubes (Figure 5A-5A'). At all-time intervals, *Sam50*-deficient murine and human myotubes showed reduced OCR (Figure 5B-B'). To begin with, myotubes were allowed to operate under normal oxidative conditions, to find basal OCR, which was impaired upon loss of *Sam50* (Figure 5C-C'). Oligomycin was then applied to inhibit ATPase and cause hyperpolarization of the membrane, which allows for ATP-linked to be understood (Figure 5D-D'). Carbonyl cyanide-4 (trifluoromethoxy) phenylhydrazone (FCCP) was then applied as an uncoupling agent mitochondrial oxidative phosphorylation to show that under conditions of maximal respiration OCR is reduced with loss of *Sam50* (Figure 5E-E'). Finally, antimycin-a and rotenone inhibit electron transport, which allows for the glycolytic reserve to be determined as a function between maximum OCR and baseline OCR (Figure 5F-F'). Together, these results show that oxidative capacity is further impaired upon ablation of *Sam50* in murine and human myotubes.

Sam50-deficiency in Murine Myotubes Changes Metabolomic Pathways

Given the association of *Sam50* with the MICOS complex, it was expected that mitochondrial structure may be dependent on it. However, the specific biochemical changes that may be occurring upon the loss of *Sam50* remains poorly elucidated. To observe changes in metabolism upon loss of Sam50, we used Gas Chromatography-Mass Spectrometry-based

metabolomics. Using a volcano plot, we noted that ß-alanine, gamma aminobutyric acid (GABA), and hypotaurine all were significantly downregulated upon loss of *Sam50* (Figure 6A). Heat map analysis shows the downregulation of various metabolites including many amino acids such as glutamine, phenylalanine, glutamate, threonine, and proline. This suggests an uptick in amino acid metabolism resulting in fewer amino acid products. In contrast, there is upregulation of ribose, ß-Hydroxy, indolepropionic, inotisol, and dihydrophenylalanine (Figure 6B). Enrichment analysis further validates these results, as the most statistically significant in amino acid and fatty acid metabolism and degradation. Beyond this, the metabolomic analysis revealed an increase in amino acid metabolism and fatty acid metabolism (Figure 6C). Together, these suggest altered biochemical pathways may arise in response, or as a mechanism of action, of altered mitochondria 3D structures upon loss of *Sam50*.

Discussion:

Together, these data suggest Sam50 is critical for the establishment and maintenance of mitochondria, mitochondrial cristae structure, and mitochondrial metabolism. To our knowledge, we are the first group to look at the 3D structure of mitochondria in murine and human myotubes following the genetic knockdown of *Sam50*. Previously, transmission electron microscopy has been utilized to observe that Sam50 can be used as a therapeutic target, with overexpression rescuing mitochondrial morphology upon injury-induced loss of morphology (47). Interestingly, our results show that *Sam50* may be functionally required for many of the diverse phenotypes previously observed in other tissue types (8). Loss of *Sam50*, importantly, showed a loss of mitochondrial morphology diverse, which may have functional impacts on functions including calcium homeostasis and mitochondria-organelle contacts.

Previously, studies have shown that Sam50 levels may rise in response to mitochondrial dysfunction, suggesting it acts as a sort of recovery molecule (47). This highlights the importance to understand how Sam50 interacts with the MICOS complex to influence overall mitochondrial structure. While it is well understood that the MICOS structure modulates cristae changes, here we also show a differential response in mitochondria structure upon loss of the SAM complex. This suggests that the MICOS complex may also affect overall mitochondrial dynamics, potentially through the modulation of fusion and fission dynamics such as Drp-1 and Opa-1, which also affects cristae structure (13). Future experiments may look at cristae to understand how cristae structural rearrangement alters 3D mitochondrial general phenotype in the loss of the MIB complex. Therefore, future experiments should consider further utilizing focused ion beam-scanning electron microscopy, which allows for machine-learning outputs of 3D cristae morphology to be constructed (33,48,49).

Importantly, our results show the importance of understanding the functional impact of mitochondria decreasing in elongation. Past studies have shown that mitochondrial with elongation may be indicative of reduced fission dynamics, such as due to loss of Drp1 (50). Mitochondria dysfunction may also arise as a result of mtDNA mutations (7). Interestingly, in an Drp1-dependent manner mtDNA mutations may cause mitochondrial morphological alterations

in Parkinson's disease; however, knockdown of Drp1 can rescue mitochondria through elongation (50). Elongated mitochondria can also serve a distinct function to distribute membrane potential across a wider area (8). Past studies have shown that loss of the mitochondrial membrane potential alters mitochondria volume (51). Membrane potential is also regulated in cristae dynamics (52). However, past research has shown that *Sam50* downregulation does not drastically alter membrane potential (26). Beyond this, it has also been suggested that elongated mitochondria offer increased ATP production and protect against mitophagy, which may aid to explain the uptick in autophagy observed following *Sam50* KO (53).

Outside of elongated mitochondria, a key mitochondrial characteristic observed exclusively in wildtype myotubes is a diversity of phenotypes. Many phenotypes have much higher complexity (Figure 3D), as well as higher surface area. This is epitomized by toroid-shaped mitochondria, which offer mitochondria an increased surface area, at the expense of volume for cristae (8). Although calcium-dependent donut mitochondria have been observed in states of ROS stress and disease (8,32), they may also serve beneficial tissue-dependent roles (54). Their absence in *Sam50-deficient* models may signify a potential inhibition of calcium. Beyond this, their increased surface area may allow wildtype myotubes to have increased contact sites with the endoplasmic reticulum, lipid droplets, and other organelles. This remains relevant as mitochondria endoplasmic reticulum sites (MERCs) serve a multitude of functions including calcium homeostasis (55,56) and regulating autophagy as autophagosomes form at ER sites (44,57). Future studies may consider further exploring this link by understanding how mitochondrial contact sites may change upon loss of *Sam50*.

Also offering valuable clues about what may be causing mitochondria function to be affected is metabolic changes we observed using GC-MS. Many of the results from the metabolic analysis show that loss of *Sam50* may result in metabolism changes that parallel disease states. For example, elevations in levels of 3,4-dihydroxyphenylalanine, which we observed increased in *Sam50*-deficient myotubes (Figure 6B), are understood to occur in association with oxidative stress during disease states (58,59). Past results have also shown that *Sam50*-deficiency is associated with liver disease through increased lipid accumulation due to increased fatty acid oxidation (60). We noted a similar effect as beta-oxidation of fatty acids increasingly occurred in *Sam50*-deficiency. In human heart, energetic demands are often carried out through the beta-oxidation of fatty acids (61). Therefore, these results suggest that it is possible that fatty acid oxidation is increased upon loss of *Sam50* to allow for energy production in states when mitochondria lose optimal functioning; however, future studies may further explore if in mitochondrial disease states, fatty acid oxidation changes in a *Sam50*-dependent manner.

Of note, we saw largely significant reductions in levels of GABA, hypotaurine, and ß-alanine in *Sam50*-deficient myotubes (Figure 6A), which may have several potential implications. Beyond functioning in embryonic neurogenesis and as a neurotransmitter, GABA acts in a potential mTOR-dependent manner with accumulation resulting in mitophagy and

abnormal morphology (62). Typically GABA is metabolized by a pathway known as the GABA shunt, found in the mitochondrial matrix; decreased frequency of GABA may be linked to upregulated upstream targets in the GABA shunt (63). It is well understood that the primary role of hypotaurine is as a precursor for taurine when reacted with hydrogen peroxide (64). Critically, taurine serves numerous functions beyond antioxidant roles, protecting against mitochondrial disease, potentially through posttranslational modifications of mitochondrial tRNAs (65,66). Together, these studies suggest a potential antioxidant role of hypotaurine in mitochondria (67). Similar to hypotaurine, ß-alanine is also a precursor to taurine production. Studies have suggested that ß-alanine supplement increases skeletal muscle carnosine content, which affects calcium homeostasis and offers antioxidant abilities, which can increase muscle endurance, yet these results remain debated (68,69). Interestingly, however, increased ß-alanine has also been shown to result in mitochondrial fragmentation and oxidative stress (70). Overall, results across prior studies show varied results suggesting a tissue-dependent role of ß-alanine which requires further elucidation.

These reductions in ß-alanine parallel a larger trend of amino acid metabolism, evidenced by decreased metabolites of many amino acids (Figure 5B). This can have numerous implications on the dependency of *Sam50* for overall mitochondrial health during disease states. For example, the catabolism of fatty acids and amino acids is commonly observed as a method to bolster cancer growth (71). These changes may also be affecting the mTORC pathway (72). Recently it was found that the mTORC pathway interacts in an OPA-1 mediated manner and may be associated with overall mitochondrial structure in stress states (73). Indeed, it has been found that the ATF4-mediated integrated stress response (ISR) is responsible for mediating cellular responses to oxidative stress and regulating amino acid metabolism (74). This pathway may be activated by ER or mitochondrial stress-dependent eIF2α phosphorylation (75). Future studies may aim to understand if metabolite pathways are changing in response to the structural-related declines in respiratory efficiency, or if the inverse is happening.

Autophagy increasingly occurring may be targeting ROS in mitochondria, which are often cause of mitophagy activation (76,77). Interestingly, past research has found that cytotoxic ROS-dependent molecules enter the mitochondria in a Sam50-mediated manner to cause ROS build-up or apoptosis (78). Therefore, loss of Sam50 may serve a cytoprotective effect by preventing apoptosis and increasing proliferation in cancer cells (79). Beyond this, *Sam50* loss also contributes to an excess of ROS species (25,79), which contribute to many pathologies. Therefore, restoring *Sam50* may act as a mechanism to prevent ROS overproduction (79) and restore mitochondrial and cristae structure (47). Our results additionally show that *Sam50* loss may further contribute to pathology through impairing mitochondrial structures, such as toroid shape and elongated mitochondria, reducing OCR, and altering metabolic pathways. Therefore, future research evaluating the targeting of *Sam50* to restore mitochondria 3D structure, function, and metabolism during *in vivo* disease states may prove a valuable future avenue.

Financial & Competing Interests' Disclosure

All authors have no competing interests.
This project was funded by the National Institute of Health (NIH) NIDDK T-32, number DK007563 entitled Multidisciplinary Training in Molecular Endocrinology to Z.V.; National Institute of Health (NIH) NIDDK T-32, number DK007563 entitled Multidisciplinary Training in Molecular Endocrinology to A.C.; Integrated Training in Engineering and Diabetes", Grant Number T32 DK101003; Burroughs Wellcome Fund Postdoctoral Enrichment Program #1022355 to D.S.; The UNCF/ Bristol-Myers Squibb (UNCF/BMS)- E.E. Just Postgraduate Fellowship in Life sciences Fellowship and Burroughs Wellcome Fund/ PDEP #1022376 to H.K.B.; NSF MCB #2011577I to S.A.M.; NSF EES2112556, NSF EES1817282, NSF MCB1955975, and CZI Science Diversity Leadership grant number 2022-253614 from the Chan Zuckerberg Initiative DAF, an advised fund of Silicon Valley Community Foundation to S.D.; The UNCF/Bristol-Myers Squibb E.E. Just Faculty Fund, Career Award at the Scientific Interface (CASI Award) from Burroughs Welcome Fund (BWF) ID # 1021868.01, BWF Ad-hoc Award, NIH Small Research Pilot Subaward to 5R25HL106365-12 from the National Institutes of Health PRIDE Program, DK020593, Vanderbilt Diabetes and Research Training Center for DRTC Alzheimer's Disease Pilot & Feasibility Program. CZI Science Diversity Leadership grant number 2022- 253529 from the Chan Zuckerberg Initiative DAF, an advised fund of Silicon Valley Community Foundation to A.H.J.; and National Institutes of Health grant HD090061 and the Department of Veterans Affairs Office of Research award I01 BX005352 (to J.G.). Additional support was provided by the Vanderbilt Institute for Clinical and Translational Research program supported by the National Center for Research Resources, Grant UL1 RR024975–01, and the National Center for Advancing Translational Sciences, Grant 2 UL1 TR000445–06 and the Cell Imaging Shared Resource. Its contents are solely the responsibility of the authors and do not necessarily represent the official view of the NIH. The funders had no role in study design, data collection and analysis, decision to publish, or preparation of the manuscript

Contributions:

ZV, KN, and EH contributed equally to this work. They performed the experimental procedures, data analysis, interpretation of results, and writing of the manuscript.

JQS, TAC, MM, and LV contributed to the experimental design and data analysis.

HB, CV, AGM, AC, and DS contributed to the data collection and analysis.

MM (McReynolds), SAM, VE, AKR, DFD, JAG, and SD provided critical feedback and contributed to the writing and revision of the manuscript.

PK and AH conceptualized the study, supervised the research, provided overall guidance, and revised the manuscript.

All authors reviewed and approved the final version of the manuscript.

Data Sharing and Open Access
All data is available upon request to the corresponding author.

Figure Legend:
Figure 1: Workflow of SBF-SEM manual contour reconstruction to create 3D mitochondrial structure upon loss of *Sam50*. (A) Workflow depicting isolation of *Sam50*-deficient human myotubes. SBF-SEM allows for (B) ortho slice alignment. (C) Manual segmentation of ortho slices was performed to (D) ultimately yield 3D reconstructions of mitochondria. (E) Once 3D reconstruction was performed, quantifications were performed for mitochondria and autophagosomes.

Figure 2: SBF-SEM shows changes in human myotubes mitochondrial 3D structure upon loss of *Sam50*. (A) Control and (B) *Sam50* knockout human myotubes orthoslice, displayed. Approximately 50 of these orthoslices are segmented to perform 3D reconstruction. (A') Control and (B') *Sam50*-deficient myotubes 3D renderings displayed overlaid on SBF-SEM orthoslice. (A'') Isolated 3D mitochondria from control and (B'') *Sam50*-deficient myotubes. (C) Upon loss of Sam50, on average mitochondria have reduced volume, (D) surface area, (E) and perimeter,

Figure 3: Changes in human myotubes mitochondrial branching and networking upon loss of *Sam50* revealed in SBF-SEM. (A) 3D Reconstructions showing control and (B) *Sam50*-deficient myotubes from a transverse-point of view. (A') 3D Reconstructions showing control and (B') *Sam50*-deficient myotubes from a longitudinal point of view. (C) Sphericity of mitochondria in control and *Sam50*-deficient myotubes. (D) Mitochondrial complexity index (MCI), which is analogous to sphericity, comparing control and *Sam50*-deficient myotubes. (E) Mito-otyping, to display the diversity of mitochondrial phenotypes as ordered by volume, in control and *Sam50*-deficient myotubes.

Figure 4: Changes in macroautophagic autophagosomes count and volume upon loss of *Sam50* revealed in human myotubes through SBF-SEM. (A) 3D Reconstruction overlaid on z-directional orthoslice of autophagosomes in control myotubes and (B) *Sam50* knockout (KO) myotubes. (A') Isolated 3D reconstruction of autophagosomes in control and (B') Sam50 KO myotubes. An uptick in macro autophagy may happen upon loss of Sam50 in myotubes, as (C) the number of autophagosomes and (D) average volume of autophagosomes increases. (E) Autophagosomes organized by the basis of their volume going from left to right to illustrate diversity of autophagic materials.

Figure 5: XF24 Seahorse Analyzer measured respiration rate. Validation through quantitative polymerase chain reaction of knockout of *Sam50*. (A) Decreased mRNA transcripts of *Sam50* in murine myotubes and (A') human myotubes following CRISPR/Cas9 transient knockout. (B) *Sam50*-deficient murine and (B') human myotubes showing reduced oxygen consumption rate (OCR) in comparison to control. (C) The first 4 time points measure basal respiration, or mitochondrial OCR at baseline in murine and (C') human myotubes. (D) The next three time points following application of oligomycin (1 µg/mL) shows decoupling of respiration dependent on ATP in murine and (D') human myotubes. (E) The next three time points measured following the addition of carbonyl cyanide 4-(trifluoromethoxy)phenylhydrazone (FCCP; 1 µM) shows OCR under maximum respiration in murine and (E') human myotubes. (F) The final three time points show OCR following rotenone (1 µM) and antimycin A (10 µM) show minimum OCR that is not dependent on mitochondria in murine and (F') human myotubes.

Figure 6: Metabolomic Comparison of *Sam50*-deficient murine myotubes and control myotubes. (A) Volcano plot of metabolites that were differentially regulated in *Sam50*-deficient myotubes compared to WT samples. (B) Relative abundance of ions in *Sam50*-deficient versus control myotubes visualized on a heatmap. (C) Enrichment analysis displaying enriched metabolites in Sam50-*deficient* myotubes.

Supplemental Figure 1:

References:

1. Alston CL, Rocha MC, Lax NZ, Turnbull DM, Taylor RW. The genetics and pathology of mitochondrial disease. *J Pathol* (2017) 241:236–250. doi: 10.1002/path.4809

2. Duchen MR, Szabadkai G. Roles of mitochondria in human disease. *Essays Biochem* (2010) 47:115–137. doi: 10.1042/bse0470115

3. Bustos G, Cruz P, Lovy A, Cárdenas C. Endoplasmic reticulum–mitochondria calcium communication and the regulation of mitochondrial metabolism in cancer: a novel potential target. *Front Oncol* (2017) 7:199.

4. Rolo AP, Palmeira CM. Diabetes and mitochondrial function: role of hyperglycemia and oxidative stress. *Toxicol Appl Pharmacol* (2006) 212:167–178.

5. Kamat PK, Kalani A, Kyles P, Tyagi SC, Tyagi N. Autophagy of Mitochondria: A Promising Therapeutic Target for Neurodegenerative Disease. *Cell Biochem Biophys* (2014) 70:707–719. doi: 10.1007/s12013-014-0006-5

6. Li L, Wu C-S, Hou G-M, Dong M-Z, Wang Z-B, Hou Y, Schatten H, Zhang G-R, Sun Q-Y. Type 2 diabetes increases oocyte mtDNA mutations which are eliminated in the offspring by bottleneck effect. *Reprod Biol Endocrinol* (2018) 16:110. doi: 10.1186/s12958-018-0423-1

7. Dabravolski SA, Orekhova VA, Baig MS, Bezsonov EE, Starodubova AV, Popkova TV, Orekhov AN. The Role of Mitochondrial Mutations and Chronic Inflammation in Diabetes. *Int J Mol Sci* (2021) 22:6733. doi: 10.3390/ijms22136733

8. Glancy B, Kim Y, Katti P, Willingham TB. The Functional Impact of Mitochondrial Structure Across Subcellular Scales. *Front Physiol* (2020) 11:541040. doi: 10.3389/fphys.2020.541040

9. Dias N, Bailly C. Drugs targeting mitochondrial functions to control tumor cell growth. *Biochem Pharmacol* (2005) 70:1–12.

10. Bratic A, Larsson N-G. The role of mitochondria in aging. *J Clin Invest* (2013) 123:951–957.

11. Cogliati S, Enriquez JA, Scorrano L. Mitochondrial cristae: where beauty meets functionality. *Trends Biochem Sci* (2016) 41:261–273.

12. Long Q, Zhao D, Fan W, Yang L, Zhou Y, Qi J, Wang X, Liu X. Modeling of Mitochondrial Donut Formation. *Biophys J* (2015) 109:892–9. doi: 10.1016/j.bpj.2015.07.039

13. C F, S C, O M de B, M M, Gv B, T R, D B, Rs P, Nn D, B DS, et al. OPA1 controls apoptotic cristae remodeling independently from mitochondrial fusion. *Cell* (2006) 126: doi: 10.1016/j.cell.2006.06.025

14. Chen H, Detmer SA, Ewald AJ, Griffin EE, Fraser SE, Chan DC. Mitofusins Mfn1 and Mfn2 coordinately regulate mitochondrial fusion and are essential for embryonic development. *J Cell Biol* (2003) 160:189–200. doi: 10.1083/jcb.200211046

15. Hu C, Shu L, Huang X, Yu J, Li L, Gong L, Yang M, Wu Z, Gao Z, Zhao Y, et al. OPA1 and MICOS Regulate mitochondrial crista dynamics and formation. *Cell Death Dis* (2020) 11:940. doi: 10.1038/s41419-020-03152-y

16. Lee H, Smith SB, Yoon Y. The short variant of the mitochondrial dynamin OPA1 maintains mitochondrial energetics and cristae structure. *J Biol Chem* (2017) 292:7115–7130. doi: 10.1074/jbc.M116.762567

17. Kühlbrandt W. Structure and function of mitochondrial membrane protein complexes. *BMC Biol* (2015) 13:1–11.

18. Kozjak-Pavlovic V. The MICOS complex of human mitochondria. *Cell Tissue Res* (2017) 367:83–93.

19. Friedman JR, Mourier A, Yamada J, McCaffery JM, Nunnari J. MICOS coordinates with respiratory complexes and lipids to establish mitochondrial inner membrane architecture. *Elife* (2015) 4:e07739.

20. Rampelt H, Zerbes RM, van der Laan M, Pfanner N. Role of the mitochondrial contact site and cristae organizing system in membrane architecture and dynamics. *Biochim Biophys Acta BBA-Mol Cell Res* (2017) 1864:737–746.

21. Anand R, Reichert AS, Kondadi AK. Emerging Roles of the MICOS Complex in Cristae Dynamics and Biogenesis. *Biology* (2021) 10:600. doi: 10.3390/biology10070600

22. Ding C, Wu Z, Huang L, Wang Y, Xue J, Chen S, Deng Z, Wang L, Song Z, Chen S. Mitofilin and CHCHD6 physically interact with Sam50 to sustain cristae structure. *Sci Rep* (2015) 5:1–11.

23. Darshi M, Taylor SS. Mitochondrial ChChD3 acts as a Scaffold for Mitofilin, Sam50 and PKA. (2008)

24. Kozjak V, Wiedemann N, Milenkovic D, Lohaus C, Meyer HE, Guiard B, Meisinger C, Pfanner N. An Essential Role of Sam50 in the Protein Sorting and Assembly Machinery of the Mitochondrial Outer Membrane *. *J Biol Chem* (2003) 278:48520–48523. doi: 10.1074/jbc.C300442200

25. Lionello S, Marzaro G, Martinvalet D. SAM50, a side door to the mitochondria: The case of cytotoxic proteases. *Pharmacol Res* (2020) 160:105196. doi: 10.1016/j.phrs.2020.105196

26. Ott C, Ross K, Straub S, Thiede B, Götz M, Goosmann C, Krischke M, Mueller MJ, Krohne G, Rudel T, et al. Sam50 Functions in Mitochondrial Intermembrane Space Bridging and Biogenesis of Respiratory Complexes. *Mol Cell Biol* (2012) 32:1173–1188. doi: 10.1128/MCB.06388-11

27. Körner C, Barrera M, Dukanovic J, Eydt K, Harner M, Rabl R, Vogel F, Rapaport D, Neupert W, Reichert AS. The C-terminal domain of Fcj1 is required for formation of crista junctions and interacts with the TOB/SAM complex in mitochondria. *Mol Biol Cell* (2012) 23:2143–2155. doi: 10.1091/mbc.E11-10-0831

28. Ott C, Dorsch E, Fraunholz M, Straub S, Kozjak-Pavlovic V. Detailed analysis of the human mitochondrial contact site complex indicate a hierarchy of subunits. *PloS One* (2015) 10:e0120213.

29. Vue Z, Garza-Lopez E, Neikirk K, Vang L, Beasley H, Marshall AG, Murray SA, Hinton Jr A. Mouse Skeletal Muscle Decrease in the MICOS Complex and Altered Mitochondrial Networks with age. *bioRxiv* (2022)2022–03.

30. Vue Z, Neikirk K, Vang L, Garza-Lopez E, Christensen TA, Shao J, Lam J, Beasley HK, Marshall AG, Crabtree A, et al. Tri-dimensional Mitochondria Reconstructions of Cardiac Muscle Changes in Size Across Aging due to the MICOS Complex. (2022)2022.04.23.489291. doi: 10.1101/2022.04.23.489291

31. Javadov S, Chapa-Dubocq X, Makarov V. Different approaches to modeling analysis of mitochondrial swelling. *Mitochondrion* (2018) 38:58–70. doi: 10.1016/j.mito.2017.08.004

32. Ahmad T, Aggarwal K, Pattnaik B, Mukherjee S, Sethi T, Tiwari B, Kumar M, Micheal A, Mabalirajan U, Ghosh B, et al. Computational classification of mitochondrial shapes reflects stress and redox state. *Cell Death Dis* (2013) 4:e461. doi: 10.1038/cddis.2012.213

33. Garza-Lopez E, Vue Z, Katti P, Neikirk K, Biete M, Lam J, Beasley HK, Marshall AG, Rodman TA, Christensen TA, et al. Protocols for Generating Surfaces and Measuring 3D Organelle Morphology Using Amira. *Cells* (2022) 11:65. doi: 10.3390/cells11010065

34. Vincent AE, White K, Davey T, Philips J, Ogden RT, Lawless C, Warren C, Hall MG, Ng YS, Falkous G, et al. Quantitative 3D Mapping of the Human Skeletal Muscle Mitochondrial Network. *Cell Rep* (2019) 26:996-1009.e4. doi: 10.1016/j.celrep.2019.01.010

35. Smolina N, Kostareva A, Bruton J, Karpushev A, Sjoberg G, Sejersen T. Primary Murine Myotubes as a Model for Investigating Muscular Dystrophy. *BioMed Res Int* (2015) 2015:e594751. doi: 10.1155/2015/594751

36. Boldrin L, Muntoni F, Morgan JE. Are Human and Mouse Satellite Cells Really the Same? *J Histochem Cytochem* (2010) 58:941–955. doi: 10.1369/jhc.2010.956201

37. Aas V, Bakke SS, Feng YZ, Kase ET, Jensen J, Bajpeyi S, Thoresen GH, Rustan AC. Are cultured human myotubes far from home? *Cell Tissue Res* (2013) 354:671–682. doi: 10.1007/s00441-013-1655-1

38. Pereira RO, Tadinada SM, Zasadny FM, Oliveira KJ, Pires KMP, Olvera A, Jeffers J, Souvenir R, Mcglauflin R, Seei A. OPA 1 deficiency promotes secretion of FGF 21 from muscle that prevents obesity and insulin resistance. *EMBO J* (2017) 36:2126–2145.

39. Boudina S, Sena S, Theobald H, Sheng X, Wright JJ, Hu XX, Aziz S, Johnson JI, Bugger H, Zaha VG, et al. Mitochondrial energetics in the heart in obesity-related diabetes: direct evidence for increased uncoupled respiration and activation of uncoupling proteins. *Diabetes* (2007) 56:2457–2466. doi: 10.2337/db07-0481

40. Dranka BP, Benavides GA, Diers AR, Giordano S, Zelickson BR, Reily C, Zou L, Chatham JC, Hill BG, Zhang J, et al. Assessing bioenergetic function in response to oxidative stress by metabolic profiling. *Free Radic Biol Med* (2011) 51:1621–1635. doi: 10.1016/j.freeradbiomed.2011.08.005

41. Hinton A, Katti P, Christensen TA, Mungai M, Shao J, Zhang L, Trushin S, Alghanem A, Jaspersen A, Geroux RE. A comprehensive approach for artifact-free sample preparation and assessment of mitochondrial morphology in tissue and cultured cells. *bioRxiv* (2021)

42. Phillips MA, Arnold KR, Vue Z, Beasley HK, Garza-Lopez E, Marshall AG, Morton DJ, McReynolds MR, Barter TT, Hinton A. Combining Metabolomics and Experimental Evolution Reveals Key Mechanisms Underlying Longevity Differences in Laboratory Evolved Drosophila melanogaster Populations. *Int J Mol Sci* (2022) 23:1067. doi: 10.3390/ijms23031067

43. Li B, Tang J, Yang Q, Li S, Cui X, Li Y, Chen Y, Xue W, Li X, Zhu F. NOREVA: normalization and evaluation of MS-based metabolomics data. *Nucleic Acids Res* (2017) 45:W162–W170.

44. Neikirk K, Vue Z, Katti P, Rodriguez BI, Omer SA, Shao J, Christensen T, Lopez EG, Marshall A, Palavicino-Maggio CB, et al. Systematic Transmission Electron Microscopy-Based Identification and 3D Reconstruction of Cellular Degradation Machinery. (2022)2021.09.26.461841. doi: 10.1101/2021.09.26.461841

45. Abudu YP, Shrestha BK, Zhang W, Palara A, Brenne HB, Larsen KB, Wolfson DL, Dumitriu G, Øie CI, Ahluwalia BS, et al. SAMM50 acts with p62 in piecemeal basal- and OXPHOS-induced mitophagy of SAM and MICOS components. *J Cell Biol* (2021) 220:e202009092. doi: 10.1083/jcb.202009092

46. Jian F, Chen D, Chen L, Yan C, Lu B, Zhu Y, Chen S, Shi A, Chan DC, Song Z. Sam50 Regulates PINK1-Parkin-Mediated Mitophagy by Controlling PINK1 Stability and Mitochondrial Morphology. *Cell Rep* (2018) 23:2989–3005. doi: 10.1016/j.celrep.2018.05.015

47. Yin X, Wang J, Yang S, Li H, Shen H, Wang H, Li X, Chen G. Sam50 exerts neuroprotection by maintaining the mitochondrial structure during experimental cerebral ischemia/reperfusion injury in rats. *CNS Neurosci Ther* (2022) 28:2230–2244. doi: 10.1111/cns.13967

48. Vidavsky N, Akiva A, Kaplan-Ashiri I, Rechav K, Addadi L, Weiner S, Schertel A. Cryo-FIB-SEM serial milling and block face imaging: Large volume structural analysis of biological tissues preserved close to their native state. *J Struct Biol* (2016) 196:487–495. doi: 10.1016/j.jsb.2016.09.016

49. Marshall AG, Damo SA, Hinton A. Revisiting focused ion beam scanning electron microcopy. *Trends Biochem Sci* (2023)S0968-0004(23)00056-7. doi: 10.1016/j.tibs.2023.02.005

50. Santos D, Esteves AR, Silva DF, Januário C, Cardoso SM. The Impact of Mitochondrial Fusion and Fission Modulation in Sporadic Parkinson's Disease. *Mol Neurobiol* (2015) 52:573–586. doi: 10.1007/s12035-014-8893-4

51. Safiulina D, Veksler V, Zharkovsky A, Kaasik A. Loss of mitochondrial membrane potential is associated with increase in mitochondrial volume: Physiological role in neurones. *J Cell Physiol* (2006) 206:347–353. doi: 10.1002/jcp.20476

52. Ghochani M, Nulton JD, Salamon P, Frey TG, Rabinovitch A, Baljon ARC. Tensile forces and shape entropy explain observed crista structure in mitochondria. *Biophys J* (2010) 99:3244–3254. doi: 10.1016/j.bpj.2010.09.038

53. Putti R, Sica R, Migliaccio V, Lionetti L. Diet impact on mitochondrial bioenergetics and dynamics. *Front Physiol* (2015) 6:

https://www.frontiersin.org/articles/10.3389/fphys.2015.00109 [Accessed February 7, 2023]

54. Bleck CK, Kim Y, Willingham TB, Glancy B. Subcellular connectomic analyses of energy networks in striated muscle. *Nat Commun* (2018) 9:1–11.

55. Moltedo O, Remondelli P, Amodio G. The mitochondria–endoplasmic reticulum contacts and their critical role in aging and age-associated diseases. *Front Cell Dev Biol* (2019) 7:172.

56. Giacomello M, Pellegrini L. The coming of age of the mitochondria–ER contact: a matter of thickness. *Cell Death Differ* (2016) 23:1417–1427.

57. Axe EL, Walker SA, Manifava M, Chandra P, Roderick HL, Habermann A, Griffiths G, Ktistakis NT. Autophagosome formation from membrane compartments enriched in phosphatidylinositol 3-phosphate and dynamically connected to the endoplasmic reticulum. *J Cell Biol* (2008) 182:685–701.

58. Zhang X, Monroe ME, Chen B, Chin MH, Heibeck TH, Schepmoes AA, Yang F, Petritis BO, Camp DG, Pounds JG, et al. Endogenous 3,4-Dihydroxyphenylalanine and Dopaquinone Modifications on Protein Tyrosine: LINKS TO MITOCHONDRIALLY DERIVED OXIDATIVE STRESS VIA HYDROXYL RADICAL *. *Mol Cell Proteomics* (2010) 9:1199–1208. doi: 10.1074/mcp.M900321-MCP200

59. Schoneich C, Hewarathna A, Pal R, Jiang L, Michaelis E. P 236 - Oxidative Stress Markers of Alzheimer's Disease in Peripheral Cell Mitochondria. *Free Radic Biol Med* (2017) 108:S100. doi: 10.1016/j.freeradbiomed.2017.04.321

60. Li Z, Shen W, Wu G, Qin C, Zhang Y, Wang Y, Song G, Xiao C, Zhang X, Deng G, et al. The role of SAMM50 in non-alcoholic fatty liver disease: from genetics to mechanisms. *FEBS Open Bio* (2021) 11:1893–1906. doi: 10.1002/2211-5463.13146

61. Parra V, Verdejo HE, Iglewski M, Del Campo A, Troncoso R, Jones D, Zhu Y, Kuzmicic J, Pennanen C, Lopez□Crisosto C. Insulin stimulates mitochondrial fusion and function in cardiomyocytes via the Akt-mTOR-NFκB-Opa-1 signaling pathway. *Diabetes* (2014) 63:75–88.

62. Lakhani R, Vogel KR, Till A, Liu J, Burnett SF, Gibson KM, Subramani S. Defects in GABA metabolism affect selective autophagy pathways and are alleviated by mTOR inhibition. *EMBO Mol Med* (2014) 6:551–566. doi: 10.1002/emmm.201303356

63. Ravasz D, Kacso G, Fodor V, Horvath K, Adam-Vizi V, Chinopoulos C. Catabolism of GABA, succinic semialdehyde or gamma-hydroxybutyrate through the GABA shunt impair mitochondrial substrate-level phosphorylation. *Neurochem Int* (2017) 109:41–53. doi: 10.1016/j.neuint.2017.03.008

64. Grove RQ, Karpowicz SJ. Reaction of hypotaurine or taurine with superoxide produces the organic peroxysulfonic acid peroxytaurine. *Free Radic Biol Med* (2017) 108:575–584. doi: 10.1016/j.freeradbiomed.2017.04.342

65. Jong CJ, Sandal P, Schaffer SW. The Role of Taurine in Mitochondria Health: More Than Just an Antioxidant. *Molecules* (2021) 26:4913. doi: 10.3390/molecules26164913

66. Suzuki BH. Revisiting the Model Minority Stereotype: Implications for Student Affairs Practice and Higher Education. *New Dir Stud Serv* (2002) 2002:21–32. doi: 10.1002/ss.36

67. Ubuka T, Okada A, Nakamura H. Production of hypotaurine from l-cysteinesulfinate by rat liver mitochondria. *Amino Acids* (2008) 35:53–58. doi: 10.1007/s00726-007-0633-x

68. Saunders B, DE Salles Painelli V, DE Oliveira LF, DA Eira Silva V, DA Silva RP, Riani L, Franchi M, Gonçalves LDS, Harris RC, Roschel H, et al. Twenty-four Weeks of β-Alanine Supplementation on Carnosine Content, Related Genes, and Exercise. *Med Sci Sports Exerc* (2017) 49:896–906. doi: 10.1249/MSS.0000000000001173

69. Bhattacharya TK, Pence BD, Ossyra JM, Gibbons TE, Perez S, McCusker RH, Kelley KW, Johnson RW, Woods JA, Rhodes JS. Exercise but not (–)-epigallocatechin-3-gallate or β-alanine enhances physical fitness, brain plasticity, and behavioral performance in mice. *Physiol Behav* (2015) 145:29–37. doi: 10.1016/j.physbeh.2015.03.023

70. Shetewy A, Shimada-Takaura K, Warner D, Jong CJ, Mehdi A-BA, Alexeyev M, Takahashi K, Schaffer SW. Mitochondrial defects associated with β-alanine toxicity: relevance to hyper-beta-alaninemia. *Mol Cell Biochem* (2016) 416:11–22. doi: 10.1007/s11010-016-2688-z

71. Li Z, Zhang H. Reprogramming of glucose, fatty acid and amino acid metabolism for cancer progression. *Cell Mol Life Sci* (2016) 73:377–392. doi: 10.1007/s00018-015-2070-4

72. Goberdhan DCI, Wilson C, Harris AL. Amino Acid Sensing by mTORC1: Intracellular Transporters Mark the Spot. *Cell Metab* (2016) 23:580–589. doi: 10.1016/j.cmet.2016.03.013

73. Hinton A, Katti P, Mungai M, Hall D, Koval O, Shao J, Vue Z, Christensen TA, Lopez EG, Rostami R, et al. OPA1 Downregulation in Skeletal Muscle Induces MERC formation in an ATF4-Dependent Manner. (2022)2022.09.12.507669. doi: 10.1101/2022.09.12.507669

74. Harding HP, Zhang Y, Zeng H, Novoa I, Lu PD, Calfon M, Sadri N, Yun C, Popko B, Paules R, et al. An Integrated Stress Response Regulates Amino Acid Metabolism and Resistance to Oxidative Stress. *Mol Cell* (2003) 11:619–633. doi: 10.1016/S1097-2765(03)00105-9

75. Tian X, Zhang S, Zhou L, Seyhan AA, Hernandez Borrero L, Zhang Y, El-Deiry WS. Targeting the Integrated Stress Response in Cancer Therapy. *Front Pharmacol* (2021) 12: https://www.frontiersin.org/articles/10.3389/fphar.2021.747837 [Accessed February 7, 2023]

76. Basit F, van Oppen LM, Schöckel L, Bossenbroek HM, van Emst-de Vries SE, Hermeling JC, Grefte S, Kopitz C, Heroult M, Hgm Willems P, et al. Mitochondrial complex I inhibition triggers a mitophagy-dependent ROS increase leading to necroptosis and ferroptosis in melanoma cells. *Cell Death Dis* (2017) 8:e2716. doi: 10.1038/cddis.2017.133

77. Chen G, Kroemer G, Kepp O. Mitophagy: An Emerging Role in Aging and Age-Associated Diseases. *Front Cell Dev Biol* (2020) 8: https://www.frontiersin.org/articles/10.3389/fcell.2020.00200 [Accessed December 21, 2022]

78. Chiusolo V, Jacquemin G, Yonca Bassoy E, Vinet L, Liguori L, Walch M, Kozjak-Pavlovic V, Martinvalet D. Granzyme B enters the mitochondria in a Sam50-, Tim22- and mtHsp70-dependent manner to induce apoptosis. *Cell Death Differ* (2017) 24:747–758. doi: 10.1038/cdd.2017.3

79. Capala ME, Pruis M, Vellenga E, Schuringa JJ. Depletion of SAM50 Specifically Targets BCR-ABL-Expressing Leukemic Stem and Progenitor Cells by Interfering with Mitochondrial Functions. *Stem Cells Dev* (2016) 25:427–437. doi: 10.1089/scd.2015.0151

Figure 1:

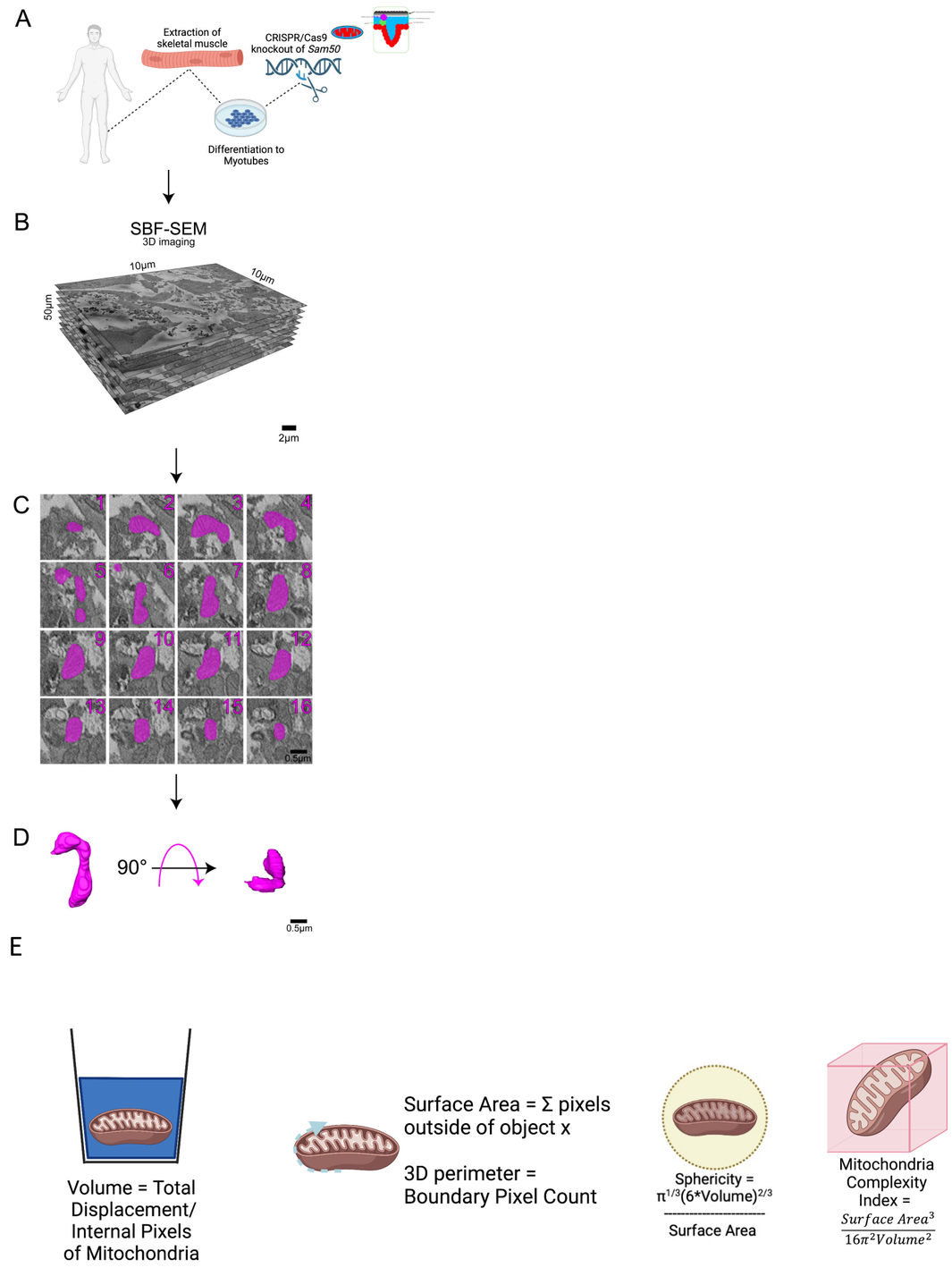
A
Extraction of skeletal muscle
CRISPR/Cas9 knockout of *Sam50*
Differentiation to Myotubes
B
SBF-SEM
3D imaging
10µm
10µm
50µm
2µm
C
0.5µm
D
90°
0.5µm
E
Volume = Total Displacement/ Internal Pixels of Mitochondria
Surface Area = Σ pixels outside of object x
3D perimeter = Boundary Pixel Count
Sphericity = $\frac{\pi^{1/3}(6*\text{Volume})^{2/3}}{\text{Surface Area}}$
Mitochondria Complexity Index = $\frac{Surface\ Area^3}{16\pi^2 Volume^2}$

Figure 2

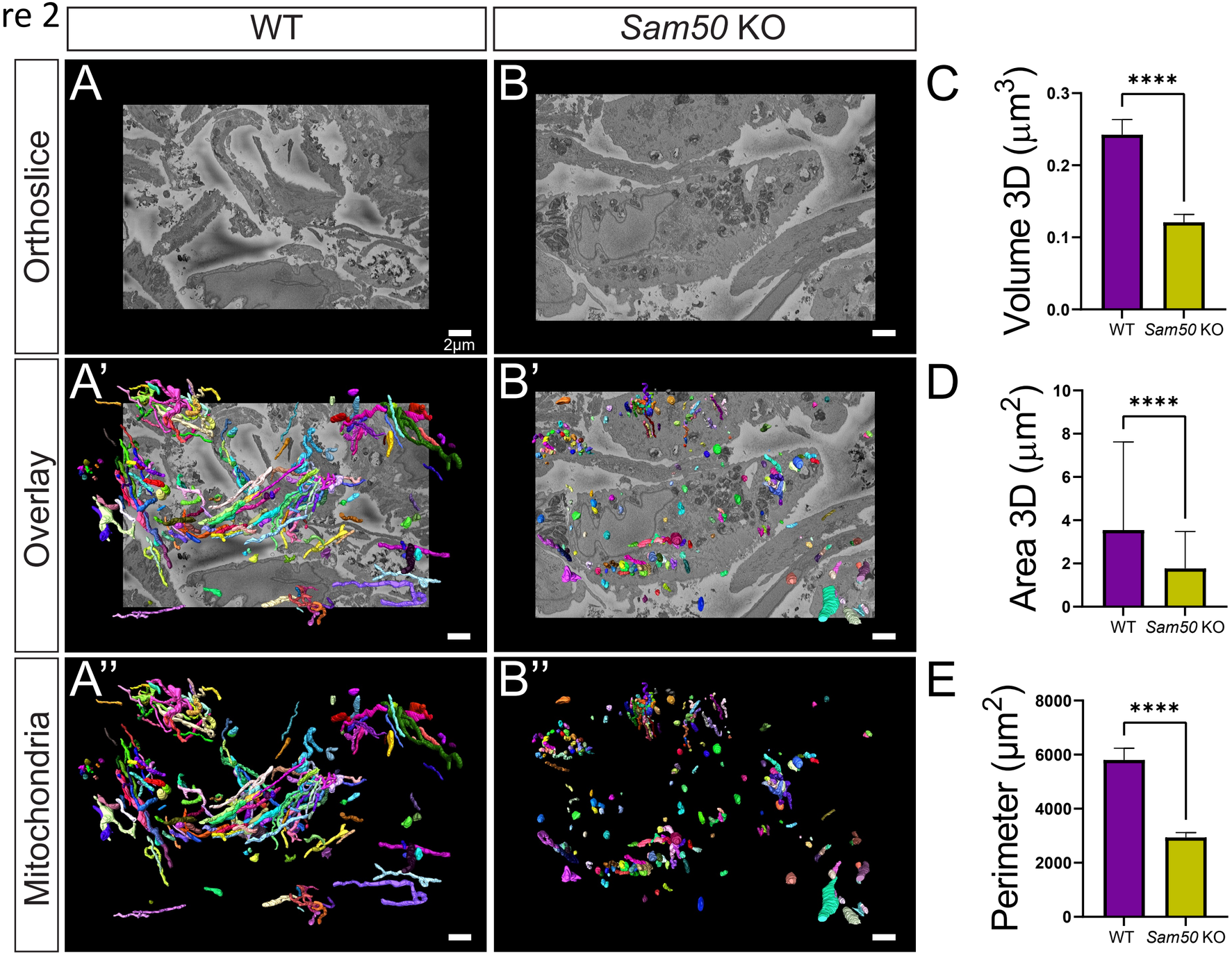
WT
Sam50 KO
Orthoslice
Overlay
Mitochondria
A
B
A'
B'
A''
B''
2µm
C
D
E
Volume 3D (µm3)
Area 3D (µm2)
Perimeter (µm2)
****
WT
Sam50 KO

Figure 3

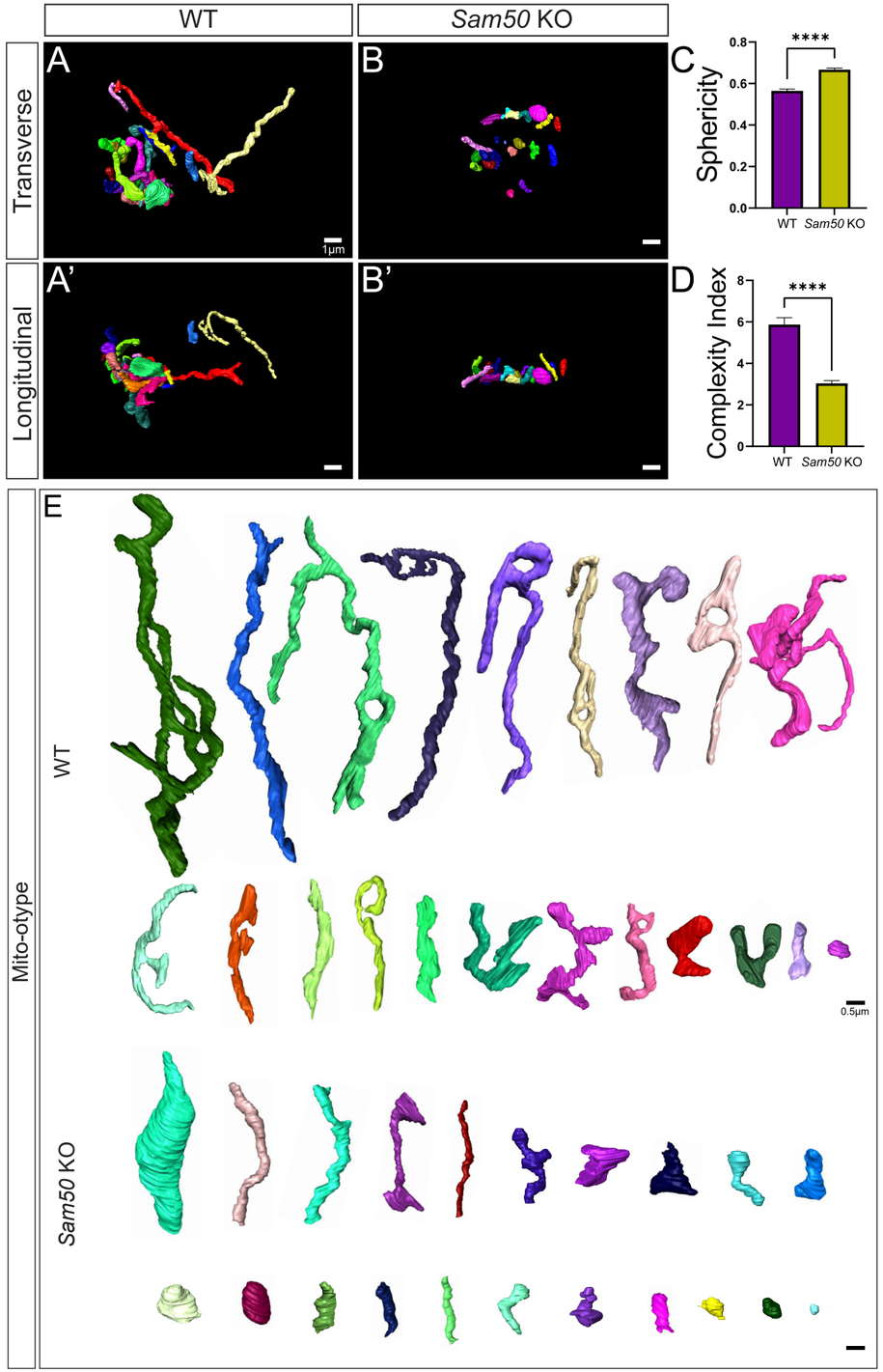
WT
Sam50 KO
Transverse
Longitudinal
A
B
A'
B'
1µm
C
Sphericity
0.8
0.6
0.4
0.2
0.0
****
WT
Sam50 KO
D
Complexity Index
8
6
4
2
0
****
WT
Sam50 KO
Mito-otype
E
WT
Sam50 KO
0.5µm

Figure 4

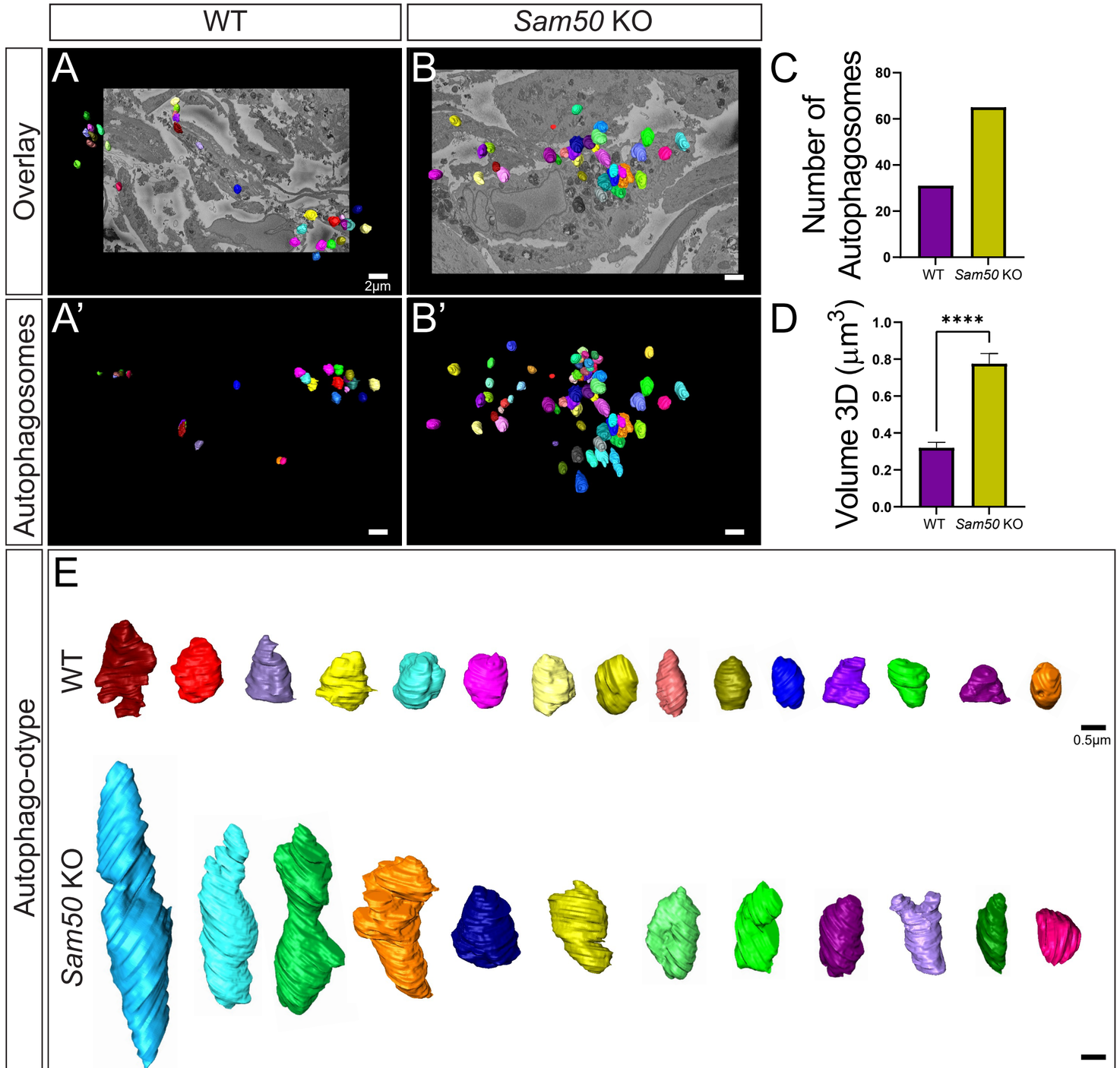
WT
Sam50 KO
Overlay
Autophagosomes
Autophago-otype
A
B
A'
B'
C
D
E
2µm
0.5µm
Number of Autophagosomes
80
60
40
20
0
WT
Sam50 KO
Volume 3D (µm3)
1.0
0.8
0.6
0.4
0.2
0.0
****
WT
Sam50 KO

Figure 5

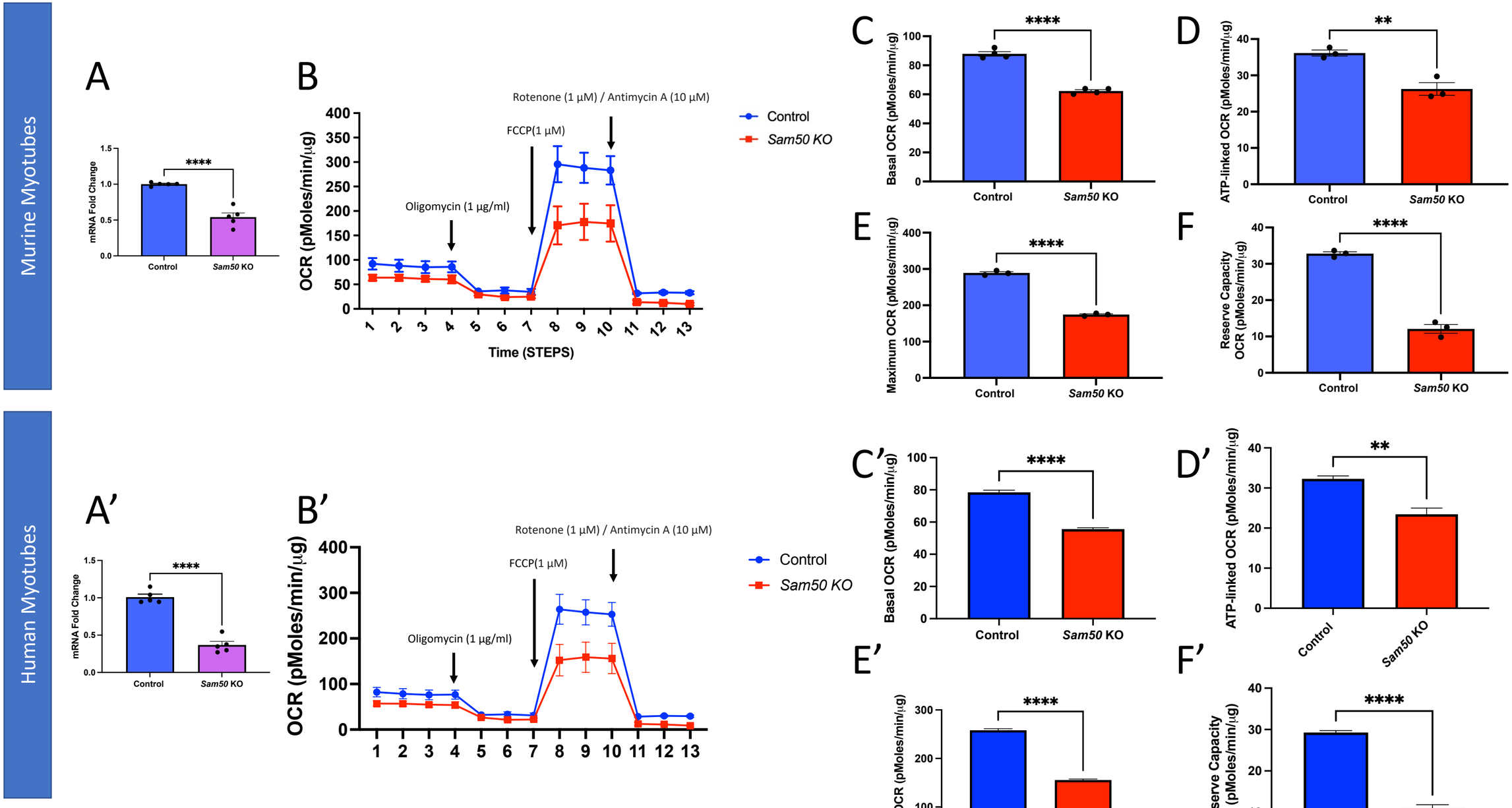
Murine Myotubes
A
mRNA Fold Change
****
Control
Sam50 KO
B
OCR (pMoles/min/µg)
Rotenone (1 µM) / Antimycin A (10 µM)
FCCP(1 µM)
Oligomycin (1 µg/ml)
Time (STEPS)
Control
Sam50 KO
C
Basal OCR (pMoles/min/µg)
D
ATP-linked OCR (pMoles/min/µg)
**
E
Maximum OCR (pMoles/min/µg)
F
Reserve Capacity OCR (pMoles/min/µg)
Human Myotubes
A'
B'
C'
D'
E'
F'

Figure 6

A

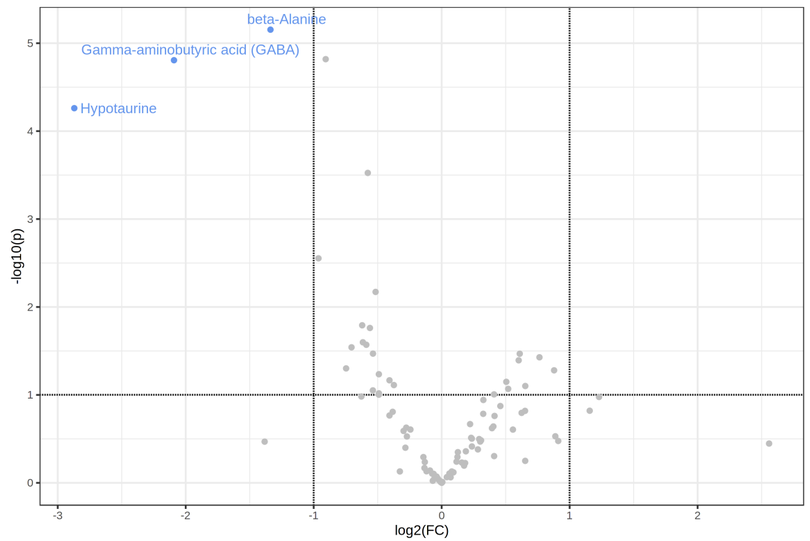
beta-Alanine
Gamma-aminobutyric acid (GABA)
Hypotaurine
-log10(p)
log2(FC)

B

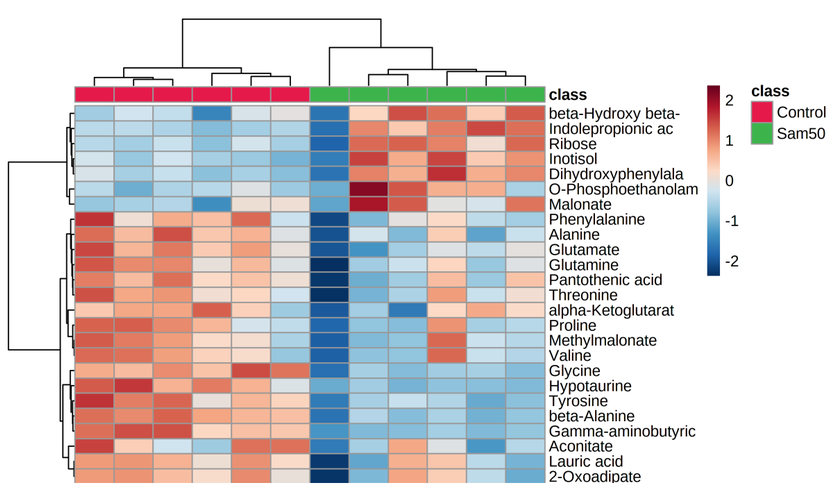
class
beta-Hydroxy beta-
Indolepropionic ac
Ribose
Inotisol
Dihydroxyphenylala
O-Phosphoethanolam
Malonate
Phenylalanine
Alanine
Glutamate
Glutamine
Pantothenic acid
Threonine
alpha-Ketoglutarat
Proline
Methylmalonate
Valine
Glycine
Hypotaurine
Tyrosine
beta-Alanine
Gamma-aminobutyric
Aconitate
Lauric acid
2-Oxoadipate
class
Control
Sam50

C

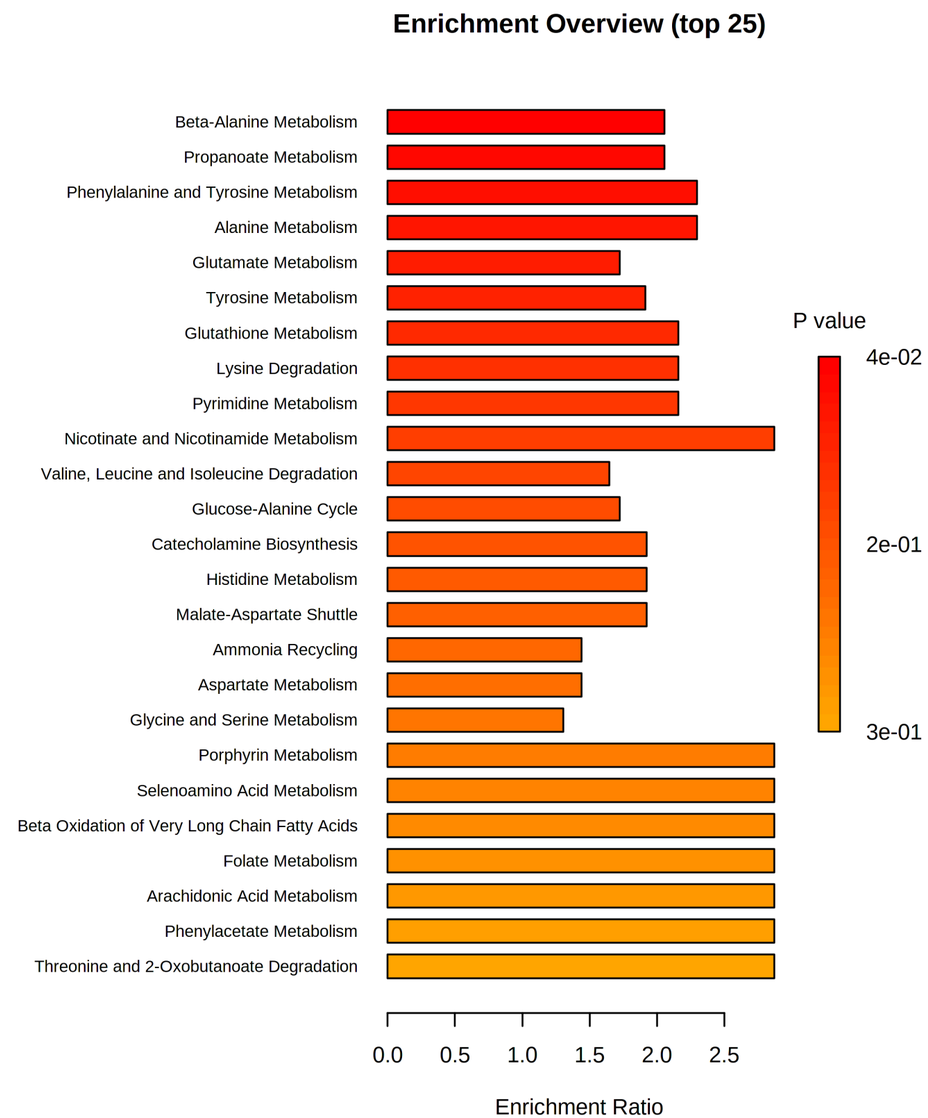
Enrichment Overview (top 25)
Beta-Alanine Metabolism
Propanoate Metabolism
Phenylalanine and Tyrosine Metabolism
Alanine Metabolism
Glutamate Metabolism
Tyrosine Metabolism
Glutathione Metabolism
Lysine Degradation
Pyrimidine Metabolism
Nicotinate and Nicotinamide Metabolism
Valine, Leucine and Isoleucine Degradation
Glucose-Alanine Cycle
Catecholamine Biosynthesis
Histidine Metabolism
Malate-Aspartate Shuttle
Ammonia Recycling
Aspartate Metabolism
Glycine and Serine Metabolism
Porphyrin Metabolism
Selenoamino Acid Metabolism
Beta Oxidation of Very Long Chain Fatty Acids
Folate Metabolism
Arachidonic Acid Metabolism
Phenylacetate Metabolism
Threonine and 2-Oxobutanoate Degradation
Enrichment Ratio
P value
4e-02
2e-01
3e-01